Effect of molecular structure on liquid slip

Ajay Vadakkepatt[*] and Yalin Dong[†]
Purdue University, West Lafayette, Indiana 47907, USA

Seth Lichter[‡]
Northwestern University, Evanston, Illinois 60208, USA

Ashlie Martini[§]
University of California Merced, Merced, California 95343, USA
(Received 27 August 2011; published 14 December 2011)

Slip behavior of three liquids with distinct molecular shapes—linear (hexadecane), branched (pentaerythritol tetra), and a chain of rings (polyphenylether)—is studied using molecular dynamics simulation and reduced-order modeling. Slip at a liquid-solid interface is shown to be affected by the molecular structure of the liquid. A two-dimensional Frenkel-Kontorova model captures the fundamental structural features of the liquid molecules and gives insight into how molecules flex and slip along the surface. We formulate an approximation to the Peierls-Nabarro energy which incorporates both the position of liquid atoms relative to substrate atoms and molecular flexibility. We find that increased molecular flexibility can lead to reduced slip by allowing the liquid to conform epitaxially to the substrate with only a small energetic penalty. Liquid molecules which are less flexible can conform to the substrate only with greater expense of conformational energy, and so exhibit larger slip.

DOI: 10.1103/PhysRevE.84.066311 PACS number(s): 47.61.−k

I. INTRODUCTION

The slip boundary condition, the quantifiable difference between velocity of a bounding wall and an adjacent liquid, has been investigated for many years using experimental methods and simulation-based techniques. Especially for nanometer-sized systems, the effect of slip can be significant. From the modeling perspective, molecular dynamics (MD) simulation has emerged as a powerful tool for investigating this behavior because, unlike continuum theory where boundary conditions are specified *a priori*, the solid-liquid velocity boundary condition is determined as a result of the MD simulation. In addition, model-predicted boundary conditions can be related directly to atomic interactions. MD simulations of interface slip typically consist of liquid molecules confined to nanoscale channels by atomically resolved walls with shear imposed either by lateral wall movement or a pressure gradient. Slip is then directly quantified as the slip velocity v_s, the difference between the wall speed and that of the adjacent liquid molecules, or the slip length L_s (to be defined later).

Slip has been found to be affected by a variety of energetic and configurational parameters [1,2]. Studies have shown slip to be affected by features of the confining walls including atomic roughness [3–6], density [7–9], and topographic structure [10–14]. On smooth surfaces, slip has been correlated to contact angle [15–17]. Modeling studies have also revealed a dependence of slip of wall-liquid interaction strength [7,8,18,19]. In this paper we focus on a less-studied topic, the role of the molecular structure of the liquid. From this perspective, the degree of branching [19–21], chain length [22,23], and the positions of single and double bonds [24] in chain polymers have been shown to play a role in slip. Correlations between molecular structure and slip have been proposed to be due to ordering effects [25] and the formation of layers of the liquid aligned near the interface [26]. Finally, the dipole moment of liquids at hydrophobic surfaces was identified as critical in determining slip [27]. A comprehensive research review on slip in thin films is available elsewhere [28].

Here, we significantly extend previous studies of liquid slip by using both MD and a reduced-order Frenkel-Kontorova (FK) model to investigate three model liquids that vary in their molecular architecture: a linear-chain hexadecane, branched pentaerythritol tetra (2-ethylhexanoate) (PEB8), and five-ring polyphenyl ether (5P4E). MD is used to relate slip to structural and energetic characteristics of the systems with focus on the structure and orientation of liquid molecules immediately adjacent to a wall. MD results are compared with the predictions of the FK model with simplified molecular configurations. It is found that the difference between unstable and stable liquid-molecule conformations defines an energy which describes the competing tendencies for the liquid to deform or epitaxially fit into the substrate. The value of this energy correlates well with a molecule's inability to slip.

II. SIMULATION DETAILS

We use nonequilibrium molecular dynamics simulations of thin liquid films in planar Couette flow as illustrated in Fig. 1. The model system consists of liquid molecules confined between two atomically smooth solid surfaces 6.4 nm apart. The length and width of the simulation cell are 6.4 × 6.4 nm and the walls are constructed of rigid atoms in an idealized face-centered-cubic (fcc) lattice with unit cell length of

[*]avadakke@purdue.edu
[†]dong5@purdue.edu
[‡]s-lichter@northwestern.edu
[§]Corresponding author: amartini@ucmerced.edu

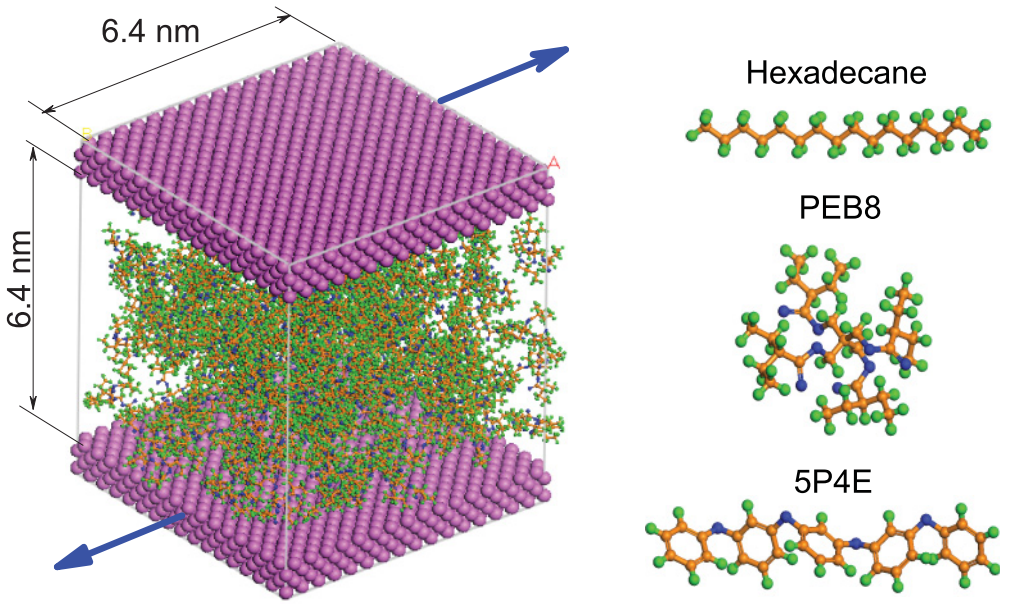

FIG. 1. (Color online) (Left) Snapshot of a molecular dynamics simulation of nano-confined liquid molecules of 5P4E sheared between fcc-structured walls. The walls are moved at constant velocity in the directions shown by the arrows. (Right) Molecular structures. Atoms are represented as spheres: orange, carbon; green, hydrogen; blue, oxygen; and pink, wall atoms. Sphere size is not representative of atomic dimensions.

0.40 nm, where the liquid interacts with the (100) plane. The three liquids studied are hexadecane, PEB8 and 5P4E. Snapshots of their molecular structures are shown in Fig. 1.

Periodic boundary conditions are applied in the flow direction and transverse to the flow along the wall. The liquid is sheared by moving the top and bottom bounding walls at equal and opposite speeds of ± 10 m/s. The polymer consistent force field (PCFF) governs both the inter- and intramolecular interactions [29]. The temperature of the liquid is maintained at 300 K using a Langevin thermostat. The initial configuration of the system is identified using Materials Studio software and all subsequent molecular dynamics simulations are performed using the LAMMPS simulation tool [30] with a time step of 1 fs for a total of 1.5 ns per simulation.

Density and velocity profiles for each case are calculated by time averaging the number and velocity of atoms in discrete bins of 0.1-nm thickness parallel to the walls. The amount of slip is quantified in terms of the slip length $L_s = v_s/\dot{\gamma}$, where v_s is the slip velocity and $\dot{\gamma}$ is the shear rate of the liquid. The shear rate is taken to be the slope of a linear fit to the average velocity profile. Slip velocity is calculated by taking the difference between the wall velocity and that of the linear profile extrapolated to a distance 0.3 nm from the wall, which is approximately one atomic diameter from the plane containing the center of masses of the interfacial solid atoms. Additional details are provided in Appendix A.

III. RESULTS

Figure 2 shows that slip lengths increase as PEB8, hexadecane, and 5P4E. The three molecules differ in the type of their constituent atoms. Most significantly, hexadecane contains only carbon and hydrogen atoms, while PEB8 and 5P4E contain oxygen as well. Oxygen has stronger van der Waals interactions than carbon. Therefore, the presence of oxygen atoms in PEB8 may lead to its having the smaller amount of slip as compared to hexadecane. We created fictitious PEB8 molecules by manually changing the interaction strength of oxygen atoms to that of carbon. The altered PEB8 has only carbon and hydrogen atoms while its shape is retained. The effect of this change on slip was found to be small. Slip for native PEB8 was 24% that of hexadecane. Replacing the oxygen atoms in the PEB8 resulted in a small increase, such that the fictitious PEB8 slip was 36% of hexadecane. If the presence of oxygen atoms was the most dominant factor, slip

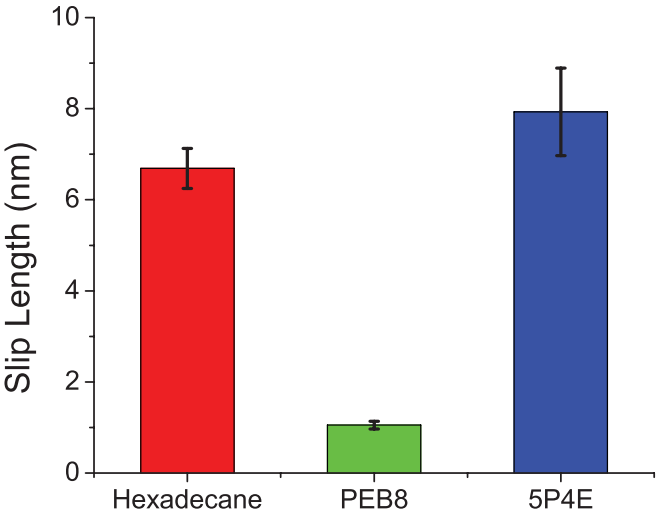

FIG. 2. (Color online) The slip length of each liquid as predicted by the molecular dynamics simulation. Error bars represent the 95% confidence interval for results from five independent simulations initialized with different atomic momenta distributions.

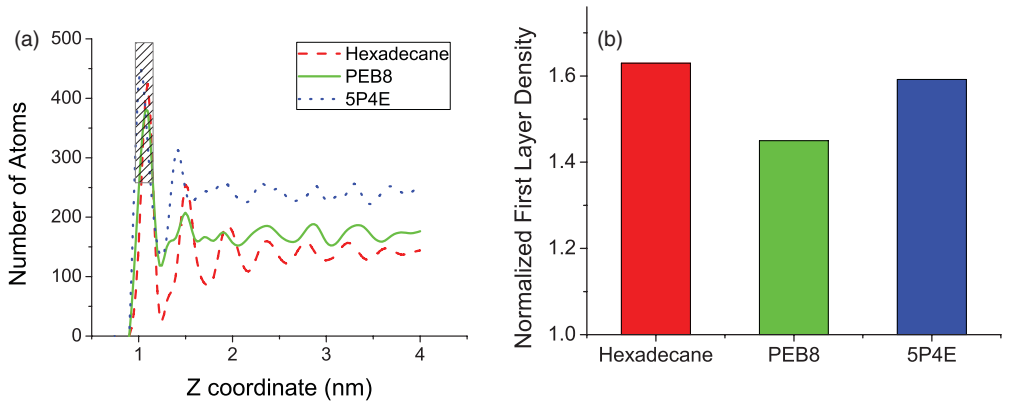

FIG. 3. (Color online) (a) Density profiles across half of the channel contrasting the molecular layering near the wall with the isotropic bulk density in the center of the channel. The first liquid layer is identified by a hatched box. (b) Density of the first liquid layer normalized by the bulk liquid density.

would have increased considerably, approaching that exhibited by hexadecane.

Density profiles averaged parallel to the walls are shown in Fig. 3(a). We observe the expected near-wall layering, exhibited as oscillations in the density profile, and the decay of these oscillations as the density becomes isotropic and approaches its bulk value. It is convenient, for use in the subsequent parts of the paper, to define the *first liquid layer* as those atoms adjacent to the wall. There is a significant difference between the bulk densities and that in the first liquid layer of all three liquids. Normalizing the first layer density by the bulk liquid density as shown in Fig. 3(b) reduces the dimensional differences from one liquid to the others, and shows that the density of the liquid in the first liquid layer is approximately 1.5 times that of the bulk density for all three liquids.

Orientation of the liquid molecules relative to the confining walls can be characterized by $S(z) = \frac{1}{2}(3\langle\cos^2\theta\rangle - 1)$, where z is the position of the center of mass and θ is the angle between the bond vector and the z axis such that $-0.5 \leqslant S \leqslant 1.0$ (only bonds between heavy atoms, i.e., carbon or oxygen, are included in the calculation). A value of -0.5 indicates the molecules are parallel to the walls, 1.0 indicates molecules are perpendicular to the walls, and 0 corresponds to no consistent ordering. The orientation parameter distributions for each liquid as well as a comparison of the orientation parameters in the first liquid layer are given in Fig. 4. As expected [22], we find that, for all fluids, the molecules are most aligned with the wall, with negative orientation parameter, in the first liquid layer. The density and orientation profiles indicate a highly dense region of aligned molecules near the wall.

We visually analyze the positions and orientations of the molecules in the first layer with respect to the placement of wall atoms. The model snapshots shown in this section are from a single moment of simulation time but are consistent with what we observe at other times. Figure 5 shows the distribution of the atoms. More detailed information is available in Fig. 6 which contains snapshots of individual liquid molecules as viewed from the top and side relative to the wall.

Figures 5(a), 6(a), and 6(d) illustrate that hexadecane molecules tend to lie flat along the wall and that they are aligned at 45° from the direction of flow. Figures 5(b), 6(b), and 6(e) show the structure of PEB8 consisting of four "legs" where, at any given time, two legs are aligned with the wall. Figures 5(c), 6(c), and 6(f) indicate that the majority of the rings in the five-ring 5P4E chain lie flat against the wall. These

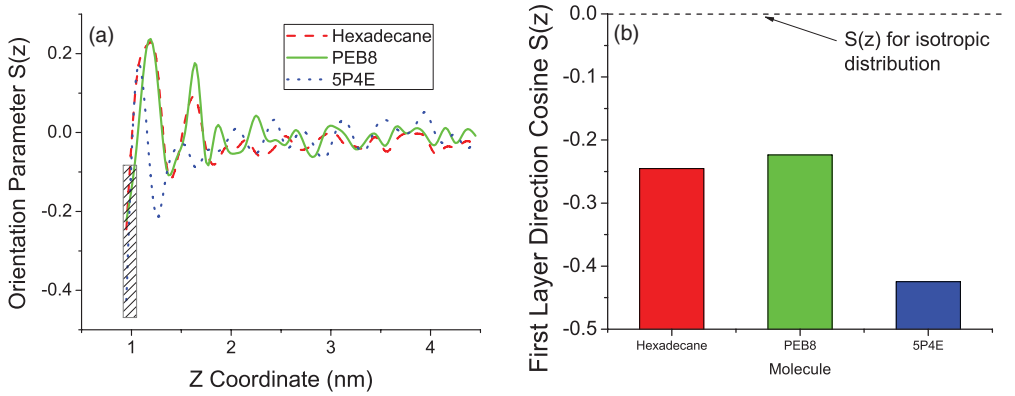

FIG. 4. (Color online) (a) Orientation parameter for the three fluids across half the channel (where the first liquid layer is identified by a hatched box), and (b) the first liquid layer.

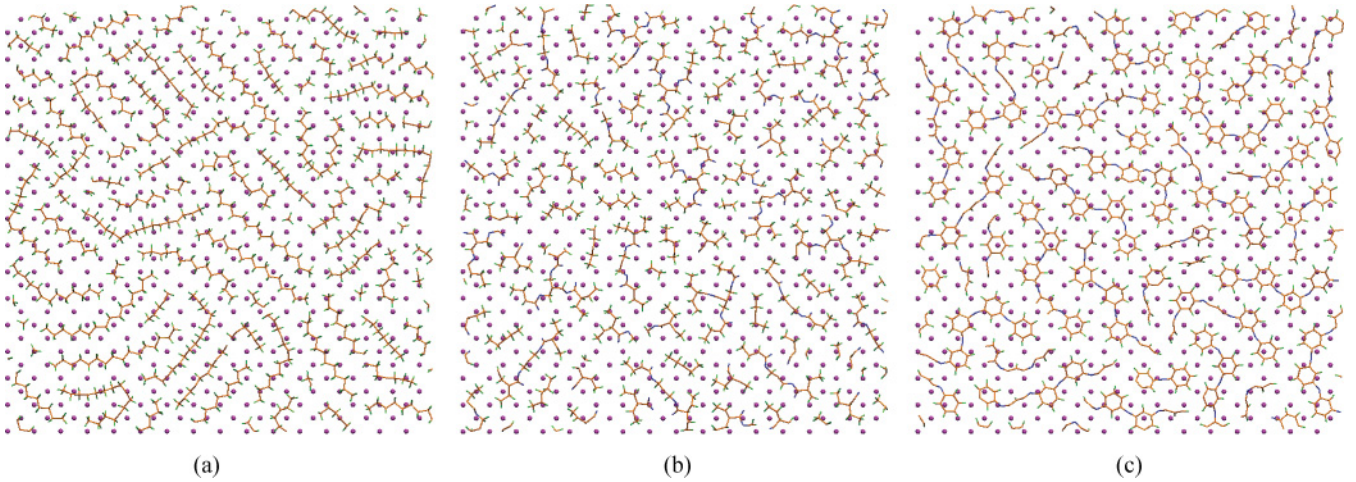

FIG. 5. (Color online) First liquid layer of (a) hexadecane, (b) PEB8, and (c) 5P4E and the adjacent wall atoms at a representative moment of time. The liquid is represented by rods, using the atomic color scheme specified in the caption to Fig. 1. Solid circles show the (100) positions of the interfacial wall atoms.

images confirm, as characterized by the negative orientation parameter, that all or part of each of the three liquid molecules tend to be aligned parallel to the wall.

In developing the reduced-order model to be discussed below, the bulk fluid is reduced to a single layer interchanging momentum with the first liquid layer. To support this simplification, we calculated the total interaction energy between the atoms in this layer and the wall, the second liquid layer (i.e., the layer defined by the second peak in the density profiles), and the bulk of the liquid. Figure 7 shows the time-averaged energy experienced by the first liquid layer. For all three molecules, we observe that the interaction between the wall and first liquid layer is much stronger than that between the liquid molecules themselves. Furthermore, the magnitude of the difference between the energy of the first and second liquid layers is only slightly more than the magnitude of the energy between the first liquid layer and all other liquid molecules indicating that viscous shear can be attributed primarily to interaction between the first and second liquid layer.

IV. DISCUSSION

A. Reduced-order modeling

Reduced-order models complement MD simulations. While MD simulations yield precise and detailed data, coarse-grained models simplify the analysis in order to evaluate the role of competing influences and identify those that are preeminent.

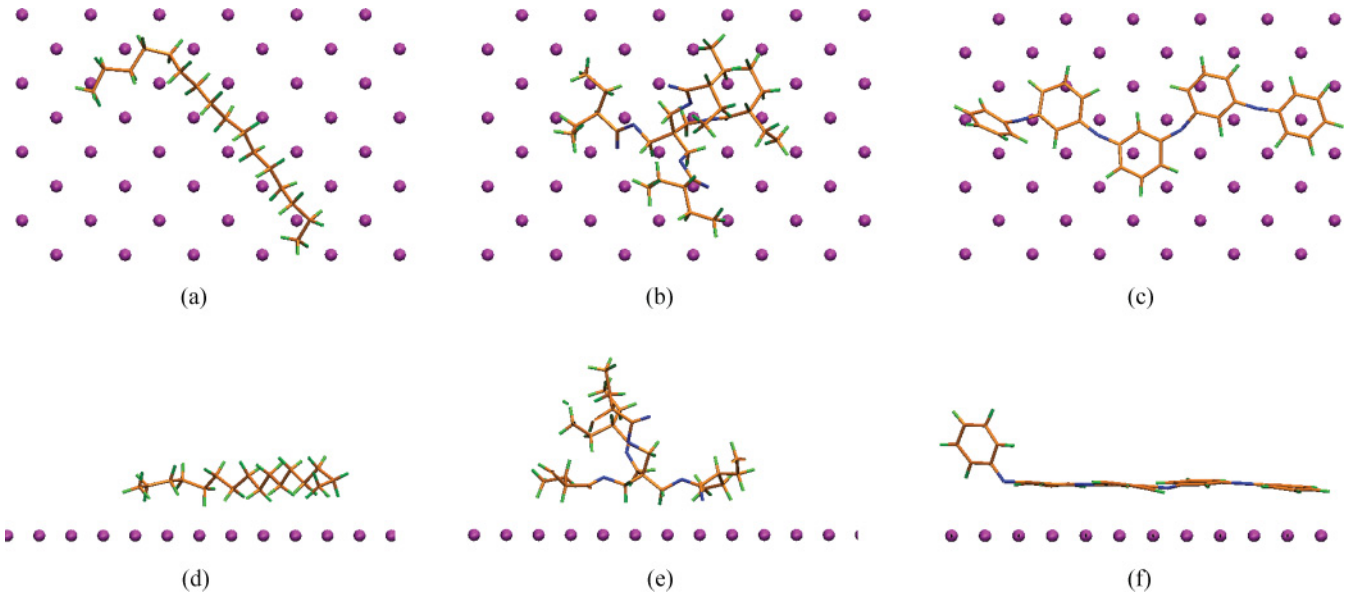

FIG. 6. (Color online) Top and side views of single hexadecane (a) and (d), PEB8 (b) and (e), and 5P4E (c) and (f) molecules and the adjacent wall atoms. The liquid is represented by rods, using the atomic color scheme specified in the caption to Fig. 1. Solid circles show the (100) positions of the interfacial wall atoms.

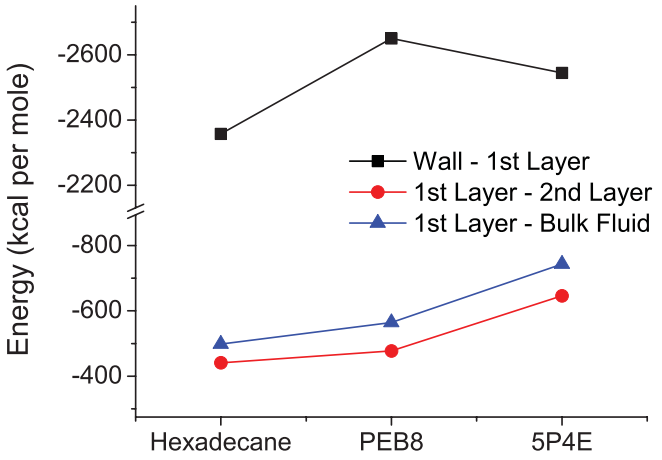

FIG. 7. (Color online) Average interaction energy between the liquid atoms in the first liquid layer and the wall (black squares), second liquid layer (red circles), or bulk of the liquid (blue triangles).

We introduce a variation of a well-known simplification of wall and liquid molecular structure known as the Frenkel-Kontorova (FK) model [31–33]. The FK model is most often implemented in its one-dimensional (1D) form, in which the two-dimensional (2D) wall is reduced to a line. Our work differs from most, in its use of the *two-dimensional* FK model which more accurately represents the substrate, the flexibility of liquid structures, and the matching of the liquid geometry to the substrate's atomic spacing.

Figure 8 can be referred to for definitions of the FK-model parameters. The bond interaction between atoms within a liquid molecule is modeled by a harmonic spring with spring constant k_b and equilibrium distance b. The angle between two adjacent bonds is restricted by another harmonic spring with constant k_n.

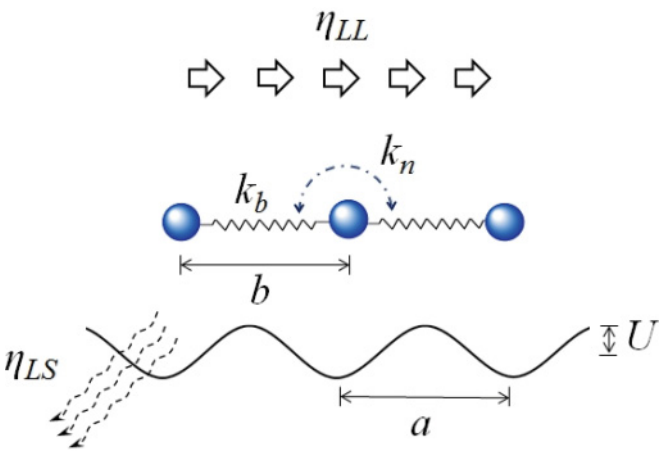

FIG. 8. (Color online) Schematic of the Frenkel-Kontorova model that simplifies a liquid-solid interface as a first liquid layer of atoms (blue spheres) interacting with a sinusoidal potential energy distribution representing the solid substrate. The bulk liquid, moving a speed v, exerts a force $\eta_{\mathrm{LL}}(v-\dot{x})$ on the first liquid layer; the substrate exerts drag force $-\eta_{\mathrm{LS}}\dot{x}$. Other parameters are defined in the text.

The interaction between an atom and the wall is represented by a sinusoidal potential energy landscape with wavelength a and amplitude U. The total potential energy of the system $V(\mathbf{x},t)$ is given by the sum of all energetic contributions,

$$V(\mathbf{x},t) = V_{\mathrm{wall}}(\mathbf{x},t) + V_{\mathrm{bond}}(\mathbf{x},t) + V_{\mathrm{angle}}(\mathbf{x},t), \qquad (1)$$

where $\mathbf{x}$ is the vector position of the atoms and t is time. The total energy consists of the following terms: V_{wall}, the energy of interaction between a liquid atom and the sinusoidal potential energy landscape; V_{bond}, the energy associated with atomic bonding; and V_{angle}, the energy due to the relative orientation between adjacent bonds. The formulation of each of the energy terms is given in Appendix B. Neglecting the thermal background, the dynamics of each atom can be described by the equation,

$$m\ddot{x}_i + \eta_{\mathrm{LS}}\dot{x}_i - \eta_{\mathrm{LL}}(v-\dot{x}_i) = -\frac{\partial V(\mathbf{x},t)}{\partial x_i}, \qquad (2)$$

where m is mass, η_{LS} is an effective friction coefficient through which momentum is transferred to the wall, and x_i, $\dot{x}_i$, and $\ddot{x}_i$ are the position, velocity, and acceleration of atom $i = 1,\ldots,N$ at time t. Shear is imposed on the atoms through the term $\eta_{\mathrm{LL}}(v-\dot{x}_i)$ which models viscous drag between liquid layers where η_{LL} is a measure of viscosity of the liquid and v is velocity. The FK-model parameters are given in Appendix B. We nondimensionalize Eq. (2) using length and time scales of $a/2\pi$ and $a/2\pi\sqrt{(m/U)}$ which results in

$$\ddot{\tilde{x}}_i = -\frac{\partial \tilde{V}}{\partial \tilde{x}_i} + \tilde{f} - \tilde{\eta}\dot{\tilde{x}}_i. \qquad (3)$$

The term $\tilde{\eta}$ is a measure of the total dissipation where $\tilde{\eta} = \tilde{\eta}_{\mathrm{LL}} + \tilde{\eta}_{\mathrm{LS}}$, and $\tilde{f} = \tilde{\eta}_{\mathrm{LL}}\tilde{v}$ is the strength of the forcing due to the bulk liquid. (For details of the nondimensionalization, please refer to Refs. [32,33].)

In order to capture the structure of the liquid molecules modeled in MD, we abstract their shapes into simple geometries as shown in Fig. 9. The atoms forming these simple geometries are connected by harmonic springs with natural length set to the bond length. As shown in Fig. 9, hexadecane is described by a linear chain of atoms, a single ring of the 5P4E molecule is mimicked by a hexagonal ring of atoms, and two triangular structures model one leg of the PEB8. The design of these simple models is motivated by the visual analysis from MD simulation with focus on capturing the geometry of the atoms that tend to lie in the first liquid layer and the overall flexibility of the structure. In the following text, the three abstracted structures will be referred to as 2D-HD, 2D-5P4E, and 2D-PEB8. The motion of the molecules according to the FK model is computed by solving Eq. (3) for each atom. All three model structures consist of six atoms which interact, according to Eq. (3), with the potential energy landscape that represents the substrate surface, is driven by the forcing $\tilde{f}$, and is slowed by a drag force, due to friction with the substrate, of $-\tilde{\eta}\dot{\tilde{x}}_i$.

B. FK model predictions

Figure 10(a) shows the displacement of the centroid of each molecule as a function of time for $\tilde{f} = 1.2$. The slope of these lines is a measure of slip velocity $\tilde{v}_s$, from which we find that slip increases as 2D-PEB8 ($\tilde{v}_s = 0.42$), 2D-HD

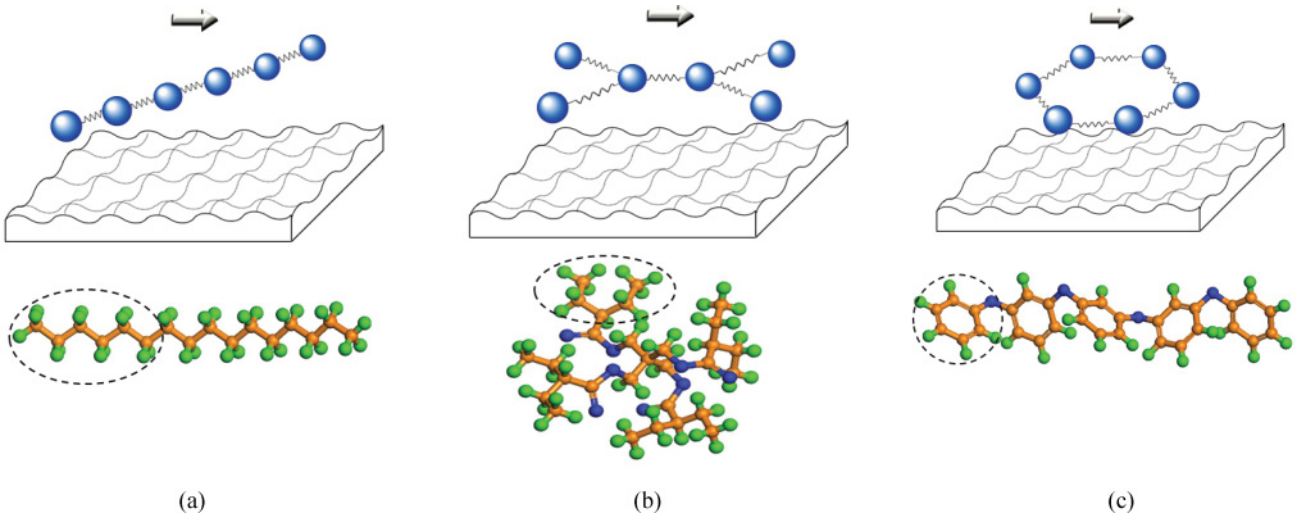

FIG. 9. (Color online) Illustration of the abstracted molecular shapes described in the FK model and their MD counterparts for (a) hexadecane, (b) PEB8, and (c) 5P4E.

($\tilde{v}_s = 0.58$), and 2D-5P4E ($\tilde{v}_s = 1.0$). This is consistent with the trend observed from the MD simulation shown in Fig. 2. The positions of the molecules relative to the 2D substrate potential are shown in Figs. 10(b)–10(d). If the molecules were point masses, we would expect them to reside nearly all the time in a potential energy well (blue in figures). However, atomic positions are constrained by the molecular configuration such that the positions we observe are affected by both the tendency to reside in potential energy wells and the restrictions to maintain molecular shape.

We sampled trajectories of the six atoms which compose each of the molecules. Figure 11(a) defines the distance from a given atom to the closest minimum of the substrate potential $V_{\text{wall}}(\mathbf{x},t)$. Figures 11(b)–11(d) show the distance as a function of time for each of the three molecules used in the FK analysis. These figures indicate the success that each atom has in residing in a low-energy position on the substrate and remaining there.

The six atoms of 2D-HD follow equivalent paths over the substrate, as indicated by their trajectories, which are identical except for a shift in time, attesting to the unchanging interatomic distances within the molecule [Fig. 11(b)]. Though the atoms spend less time in the neighborhood of higher energies, as shown by the sharp peaks, and more time near energy minima, as shown by the rounded troughs, the upper and lower halves of the trajectories are similar. Thus, the substrate potential only weakly traps the atoms which pass near. Also, as shown in Fig. 10(b), the 2D-HD molecules tend to align at 45° with respect to the surface. At low forcing ($\tilde{f} \lesssim 1.4$), we observe 2D-HD moving at 45° with respect to the direction of the applied shear stress. At higher forcing the liquid intermittently jumps over a set of wall atoms to the next low-energy region.

Compared with 2D-HD, the atomic trajectories for 2D-PEB8 show much more variability between atoms [Fig. 11(c)]. Atoms 2 and 4 have similar paths over the substrate. Both rapidly move away from high-energy locations and linger at smaller distances, with atom 4 coming closest to the energy minima. Atoms 1, 3, 5, and 6 show the opposite tendency, staying close to high-energy locations, while spending relatively less time near minima. These trajectories, compared to the other two molecules, are the most complex and variable, suggestive of a flexible molecule. This flexibility enables the molecule to reside at a favorable position on the energy landscape for a relatively long period of time.

Among the three molecules, 2D-5P4E's atom 4 both comes closest to and farthest from minima [Fig. 11(d)]. However, all atoms of 2D-5P4E spend little time near minima as shown by the sharpness of their troughs. The crests, however, are broad, especially for atoms 2 and 4. 5P4E has the widest spread in instantaneous distances among the three molecules. While one atom may find a position of low potential, the rigidity of its structure offers little opportunity for other atoms, or for that atom at another time, to avoid one high-energy site or another.

From the trajectories shown, we can compute the mean distance as the average distance over all six atoms and over the duration shown in Fig. 11. The mean distance from the nearest minima for 2D-PEB8 atoms, 0.97, is less than half that for the other two molecules, 1.96 and 2.42, for 2D-HD and 2D-5P4E, respectively. This small mean distance and the length of time spent at moderate distances suggests that 2D-PEB8 flexes to stay close to the low-potential sites along the substrate. The ringlike shape of 2D-5P4E shown in Fig. 10(d) is the most restrictive of the three molecules we have studied. As the molecule slips along the surface, there is very little variation in the shape due to the influence of the potential energy distribution. The molecule's rigidity does not allow it to reside at energetically favorable positions.

The Peierls-Nabarro energy (or Peierls-Nabarro barrier) $\tilde{V}_{\text{PN}}$ is a useful means to distinguish slippery situations, in which slip can easily occur, from stuck ones, in which slip can hardly occur, if at all [33]. Consider those potentials $\tilde{V}$ which satisfy Eq. (3) for $\ddot{\tilde{x}}_i = \dot{\tilde{x}}_i = 0$ for all atoms i. Of these stationary configurations, the one with the least energy $\tilde{V}_{\text{min}}$ defines a stable configuration. The saddle point between two adjacent stable configurations defines the unstable configuration with energy $\tilde{V}_{\text{max}}$. The difference between these two energies defines the Peierls-Nabarro energy, $\tilde{V}_{\text{PN}} = \tilde{V}_{\text{max}} - \tilde{V}_{\text{min}}$ [34].

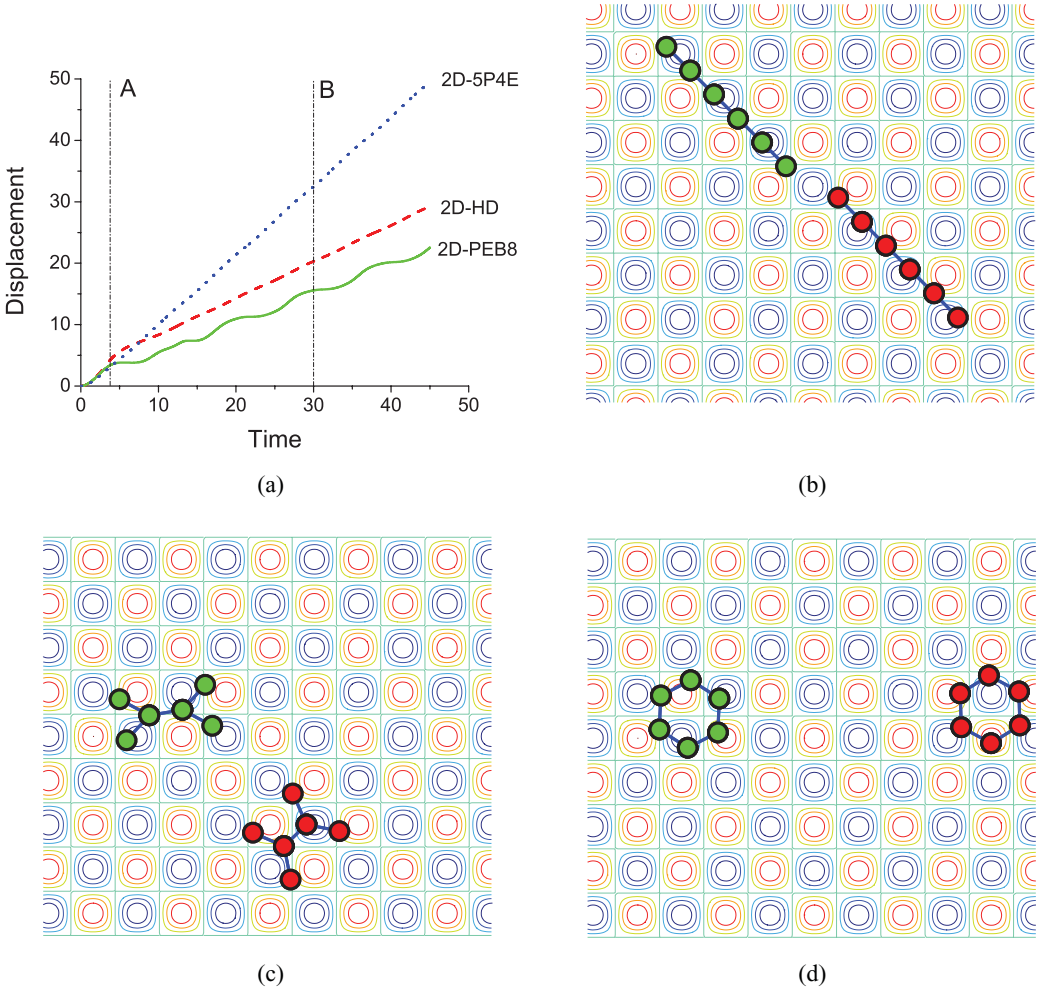

FIG. 10. (Color online) (a) Displacement as function of time for 2D-HD, 2D-PEB8, and 2D-5P4E, and (b)–(d) corresponding atomic positions for each molecule at two time steps, A and B, as indicated in (a) relative to the potential energy landscape where colors from blue to red indicate regions from low to high energy.

The energy $\tilde{V}_{\mathrm{PN}}$ is the minimum energy needed for slip to occur. On the substrate, liquid molecules in the first liquid layer can lower their energy by locating their constituent atoms at positions between substrate atoms. Consider a stiff liquid molecule whose heavy atoms (that is, those excluding hydrogen) are such that they do not register with the distance separating substrate atoms. In general, then, liquid atoms can squeeze into low-energy sites on the substrate only by increasing their conformational energy, due to stretching and rotation of bonds. For this type of molecule, $\tilde{V}_{\mathrm{PN}}$ will be small, as even the stable state will have a large energetic contribution from bond and angle energies [see Eq. (1)], and slip will occur easily. On the other hand, consider a liquid molecule whose atomic spacings match those of the substrate atoms, or whose bonds stretch and rotate easily with little change in energy. Then, the liquid can conform its atoms into low-energy sites on the substrate, achieving a low $\tilde{V}_{\mathrm{min}}$. In this case, even if the flexible liquid molecule needs to deform in order to register epitaxially with the substrate, it can do so at little increase of bond and angle energies, and so the low-energy conformation will be close to the least-possible minimum, with all atoms located at the minima of the substrate potential. The maximum energy configuration will be with the liquid atoms located nearly overhead the substrate atoms, in positions of high energy. As a result $\tilde{V}_{\mathrm{PN}}$, the difference between having all the liquid atoms at low versus high-energy positions, will be large.

The description above the Peierls-Nabarro barrier is strictly valid only for one-dimensional systems. We use it here to gain qualitative understanding of the effect of molecular flexibility on slip. We expect the closed ring structure of 5P4E to be rigid, and hence lead to a small $\tilde{V}_{\mathrm{PN}}$ and large slip. Hexadecane is expected to be less rigid, but its linear spacing of carbon atoms does not register into the low-energy sites of the substrate. Hence, for these two molecules, the difference between the stable and unstable states is expected to be small, leading to small $\tilde{V}_{\mathrm{PN}}$ and large slip. The dangling branching ends of PEB8 are more flexible, and are expected to yield a large $\tilde{V}_{\mathrm{PN}}$ and small slip. To test these ideas, for all times t during the FK simulation, the total potential $V(\mathbf{x},t)$ is measured. The Peierls-Nabarro barrier $\tilde{V}_{\mathrm{PN}}$ is approximated as the difference between the maximum and minimum value of $V(\mathbf{x},t)$ over the FK simulation, and is shown in Fig. 12. The two liquids with the larger slip lengths, namely 2D-HD and 2D-5P4E, have

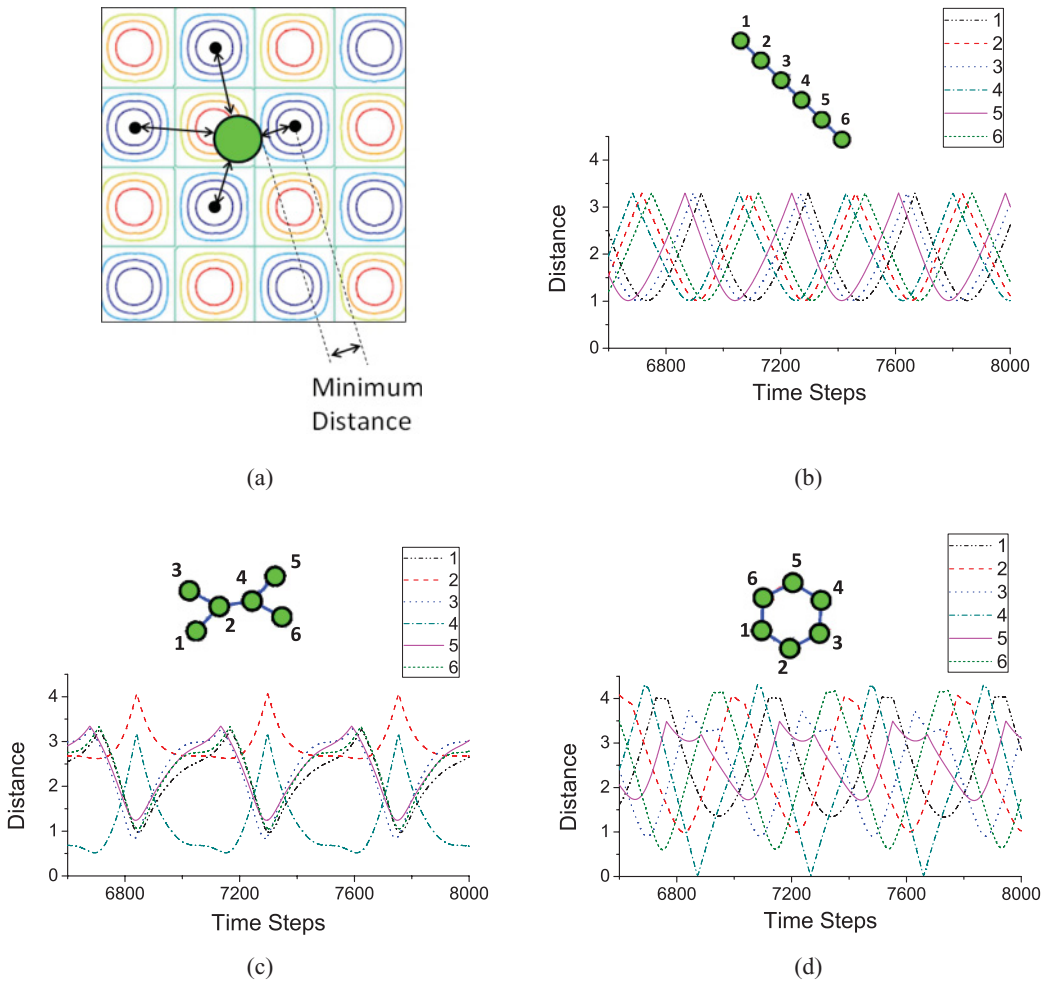

FIG. 11. (Color online) (a) The large green circle shows a representative atom from the six-atom molecules used in the FK analysis and shown in the upper part of (b)–(d). (b)–(d) The instantaneous distance of each of the numbered atoms to the closest minimum of $V_{\text{wall}}(\mathbf{x},t)$, as shown in (a). Distance has been nondimensionalized with respect to $a/(2\pi)$ and time is given in terms of the computational time step. (b) 2D-HD; (c) 2D-PEB8; (d) 2D-5P4E.

nearly equal and small values of $V(\mathbf{x},t)$ for all forcings f. However, 2D-PEB8, which is observed to hardly slip, has a much larger value of $V(\mathbf{x},t)$.

We find the following: (1) The value of $\tilde{V}_{\text{PN}}$ reflects the liquid molecule's flexibility and its commensurability with the substrate. Flexible and commensurate molecules have high values of $\tilde{V}_{\text{PN}}$, while rigid and incommensurate molecules have low values. (2) The value of $\tilde{V}_{\text{PN}}$ is correlated to the amount of slip. High (low) $\tilde{V}_{\text{PN}}$ leads to low (high) slip length.

Figure 13 illustrates slip velocity as a function of the forcing amplitude $\tilde{f}$. Slip is zero for zero forcing, as expected by symmetry, and it remains zero for a range of the lowest values of forcing. At a liquid-dependent critical force value, there is a transition to slip. To understand this, consider an FK model of a point particle over a 1D sinusoidal substrate [32]. For velocity and acceleration equal to zero, Eq. (3) simplifies to $\tilde{f} = \sin\tilde{x}$. If $\tilde{f} < 1$, then solutions exist corresponding to stable positions at which the atom can reside, and so zero slip is possible. However, as the amplitude of forcing increases, when $\tilde{f} > 1$ there are no stable solutions, which means that the slip velocity cannot be zero. Hence, in the 1D model, $\tilde{f} = 1$ is the critical forcing above which the entire first liquid layer will commence slip. From Fig. 13 we can see that the 2D model also shows a critical force above which slip commences. When expressed in terms of dimensional parameters, the critical forcing in the 1D FK model is proportional to the liquid viscosity [32]. The bulk liquid viscosities increase in the following order: hexadecane (HD), PEB8, 5P4E. This is not the order seen in Fig. 13, for which the critical forcing is approximately 0.2, 0.5, and 1.2 for 2D-HD, 2D-5P4E, and 2D-PEB8, respectively. While hexadecane does have the lowest critical forcing, the order of PEB8 and 5P4E is reversed from what is expected from the 1D analysis, which is based on the motion of a point particle. We speculate that the flexibility of the liquid molecules may also play a role in setting the critical forcing amplitude. Molecular structure may affect not only the magnitude of slip but also the critical forcing at which it first occurs.

V. CONCLUSION

In summary, we have used fully atomistic molecular dynamics simulation and the reduced-order Frenkel-Kontorova

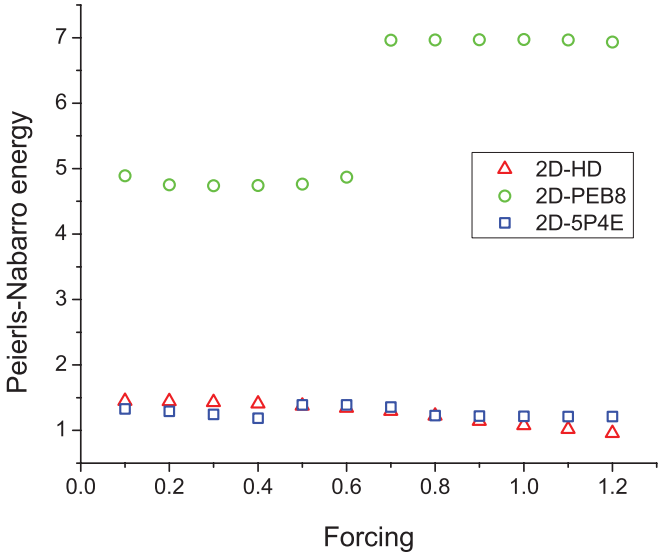

FIG. 12. (Color online) The natural log of the measured approximation to the Peierls-Nabarro energy for 2D-HD (blue triangles), 2D-PEB8 (red circles), and 2D-5P4E (black squares) versus the value of the nondimensional forcing. Low (high) Peierls-Nabarro barrier leads to large (small) values of slip length (cf. Fig. 2). The jump in energy that occurs at $0.6 < \tilde{f} < 0.7$ is due to a shift of the position of 2D-PEB8 from one quasistable position to another.

model to study liquid slip. The three molecules studied have different molecular structure. As a consequence, they exhibit different slip behavior. These differences are observed in molecular dynamics simulations in the magnitude of slip length, and the near-wall molecular density, orientation, and energy. The MD simulation results suggest that slip is due to the combined effects of wall-liquid interaction and molecular shape. In distinction with prior work on the one-dimensional FK model using point particles, we model the substrate as a two-dimensional surface and model the liquid using a simplified six-atom structure. We find that

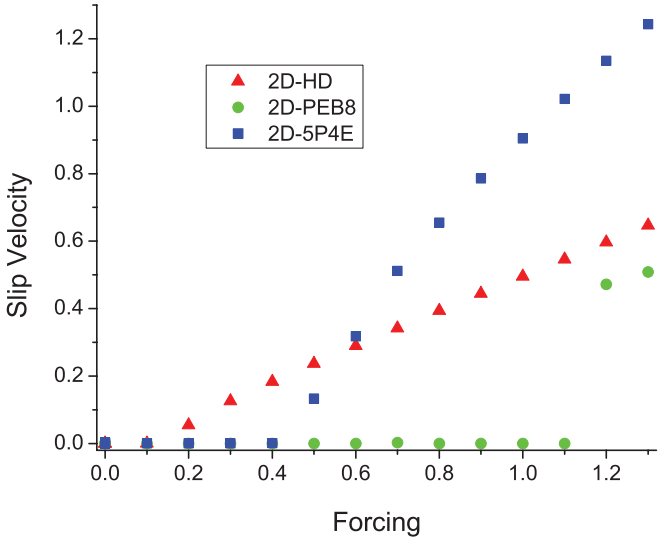

FIG. 13. (Color online) Variation of slip velocity $\tilde{v}_s$ with forcing amplitude $\tilde{f}$ for each simplified liquid molecule.

the onset of slip depends on the molecular structure of the liquid. An approximation to the Peierls-Nabarro barrier shows that molecular flexibility and position of liquid atoms relative to substrate atoms determines the amount of slip. Increased molecular flexibility can lead to reduced slip, as it allows the liquid to conform epitaxially to the substrate, with only a small energetic penalty in added conformational energy. Liquid molecules which are less flexible and which can conform to the substrate only at the expense of conformational energy, have larger values of slip. Finally, we hope that the combined techniques of MD simulation and reduced-order FK modeling will be further applied to increase our understanding of liquid slip over solid substrates, and to develop the principles which control the amount and direction of slip.

ACKNOWLEDGMENTS

A.V., Y.D., and A.M. thank the National Science Foundation for its support via Grant No. EEC-0821875. S.L. thanks the Lillian Sidney Foundation.

APPENDIX A: MD SIMULATION

In this section, we provide further implementation details for the MD simulation. The three liquids modeled are hexadecane ($C_{16}H_{34}$), pentaerythritol tetra ($C_{37}H_{68}O_8$), and polyphenyl ether ($C_{30}H_{22}O_4$). The molecular masses are 226.4, 640.9, and 446.5 grams per mole, and ambient densities 767, 954 and 1200 kg/m^3, respectively. The initial atomic positions of these molecules are created using Material Studio software using the Amorphous Cell module. As mentioned earlier, the dimensions of the simulation cell are $6.4 \times 6.4 \times 6.4$ nm which consists of two walls and the confined liquid. The walls are constructed as fcc crystals (unit cell length 0.4 nm) in the (100) orientation with cross-sectional dimensions $6.4 \times 6.4 \times 0.8$ nm. These dimensions correspond to $16 \times 16 \times 2$ unit cells and 2723 atoms per wall. For each liquid at the bulk ambient density, the number of molecules in this simulation cell are 537 for hexadecane, 285 for PEB8, and 424 for 5P4E.

The initial configurations are exported and then reformatted such that they can be input into LAMMPS software. Before shearing the liquid, the system is equilibrated during which the time-step size is gradually increased from 0.001 to 1 fs (0.5 ns at 0.001 fs, 0.5 ns at 0.01 fs, 0.5–1 ns at 0.1 fs, and 0.5–1 ns at 1 fs). Once equilibrated, the walls are given a constant velocity in equal and opposite directions to shear the fluid. During the dynamics, temperature is controlled using the Langevin thermostat at 300 K and with a damping parameter of 10 ps. This value of the damping parameter is chosen to be small enough that the thermostat does not affect the viscous properties of the fluid significantly, but large enough to control the temperature by removing the heat generated by the shear flow [24].

Velocity profiles are obtained by time averaging the velocities of bins as discussed in the text. Illustrations of these profiles for each liquid and the associated slip velocities are shown in Fig. 14. Shear rate is determined from a linear fit to the velocity profile and the slip lengths reported in Fig. 2 are obtained by dividing slip velocity by shear rate.

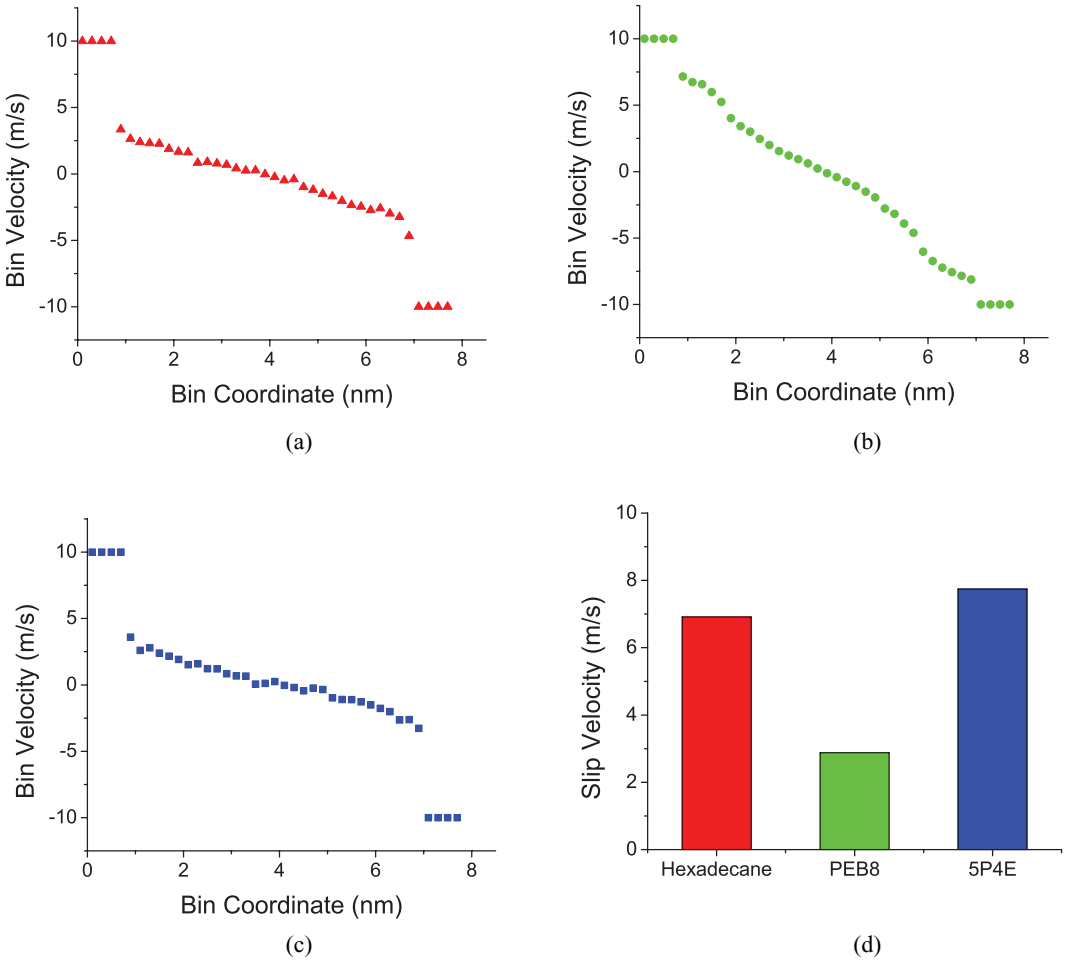

FIG. 14. (Color online) Average velocity of the liquid atoms in bins parallel to the walls for (a) hexadecane, (b) PEB8, and (c) 5P4E, and (d) the corresponding slip velocities.

APPENDIX B: FK MODEL

The following is a summary of the FK model applied to liquid slip over a two-dimensional surface. First, we derive the analytical expression for the potential corresponding to an fcc structured wall aligned in any direction in the x-y plane.

For a unit cell aligned at an angle ϕ to the x axis (Fig. 15), lattice vectors are given by

$$\mathbf{a}_1 = \begin{bmatrix} a\cos\phi \\ a\sin\phi \end{bmatrix}, \quad \mathbf{a}_2 = \begin{bmatrix} a\sin\phi \\ -a\cos\phi. \end{bmatrix}. \tag{B1}$$

The reciprocal vectors are calculated from

$$\mathbf{a}_1 \cdot \mathbf{q}_1 = 2\pi, \tag{B2}$$

$$\mathbf{a}_2 \cdot \mathbf{q}_1 = 0,$$

$$\mathbf{a}_1 \cdot \mathbf{q}_2 = 0, \tag{B3}$$

$$\mathbf{a}_2 \cdot \mathbf{q}_2 = 2\pi.$$

Solving for q_1 and q_2, the reciprocal vectors are given by

$$\mathbf{q}_1 = \begin{bmatrix} \frac{2\pi}{a}\cos\phi \\ \frac{2\pi}{a}\sin\phi \end{bmatrix}, \quad \mathbf{q}_2 = \begin{bmatrix} \frac{2\pi}{a}\sin\phi \\ -\frac{2\pi}{a}\cos\phi \end{bmatrix}, \tag{B4}$$

where $\phi = 45^\circ$ for a wall orientation consistent with that of the MD simulation.

An approximate form for the corrugation potential V_{wall} is given by the first term of the two-dimensional Fourier series of the primitive lattice vectors and has the form [15,35],

$$V_{\text{wall}}(\mathbf{x},t) = U_c + U\sum_{i}^{N}(\cos(\mathbf{q}_1 \cdot \mathbf{x}_i) + \cos(\mathbf{q}_2 \cdot \mathbf{x}_i)). \tag{B5}$$

The bond potential is given by

$$V_{\text{bond}}(\mathbf{x},t) = \sum_{i=1}^{N}\sum_{j=1}^{M_i}\frac{1}{2}k_b(\Delta\mathbf{x}_{ij} - b)(\Delta\mathbf{x}_{ij} - b), \tag{B6}$$

where b represents the equilibrium bond length between the i^{th} and j^{th} atoms, M_i represents the number of atoms connected to the i^{th} atoms through bonds and $\Delta\mathbf{x}_{ij} = \mathbf{x}_i - \mathbf{x}_j$.

The angle potential is given by

$$V_{\text{angle}}(\mathbf{x},t) = \sum_{i=1}^{N}\sum_{j=1}^{P_i}\frac{1}{2}k_n(\theta - \theta_0)^2, \tag{B7}$$

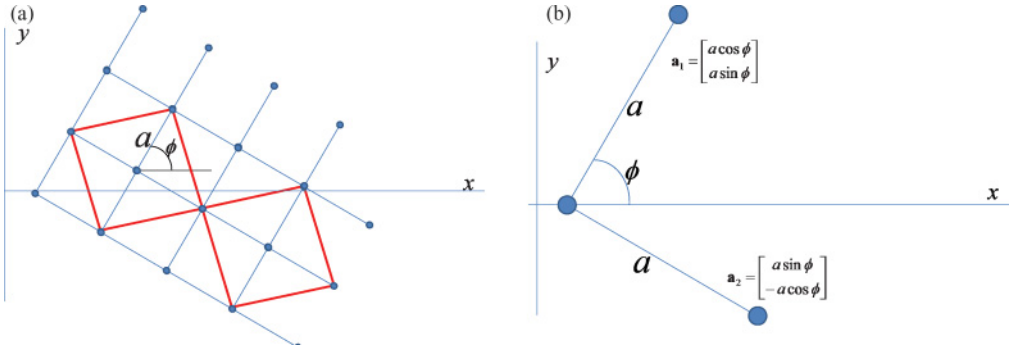

FIG. 15. (Color online) Illustration of lattice vectors. (a) Red rectangle representing unit cell and (b) lattice vectors.

where θ and θ_0 are the instantaneous and equilibrium angles between the two bonds forming the angle and P_i represents the number of angles for the i^{th} atom. The instantaneous angle is calculated by

$$\theta = \frac{\langle \Delta\mathbf{x}_{ik}, \Delta\mathbf{x}_{il} \rangle}{|\Delta\mathbf{x}_{ik}||\Delta\mathbf{x}_{il}|}, \tag{B8}$$

where $\Delta\mathbf{x}_{il}$ and $\Delta\mathbf{x}_{il}$ are the bond vectors.

The FK-model parameters were chosen to be consistent with the MD simulations: $m = 12.01$ amu (mass of a carbon atom), $k_b = 299.67\,\text{kcal/mol/Å}^2$ (C-C bond coefficient), $k_n = 41.4530\,\text{kcal/mol/rad}^2$ (C-C-C angle coefficient), $b = 1.53$ Å (C-C bond coefficient), $a = 4/\sqrt{2}$ Å (atomic distance), and $U = 1$ kcal/mol.

The resulting set of coupled differential equations are solved using the fourth-order Runge-Kutta method.

[1] S. Lichter, A. Martini, R. Q. Snurr, and Q. Wang, Phys. Rev. Lett. **98**, 226001 (2007).
[2] A. Martini, H.-Y. Hsu, N. A. Patankar, and S. Lichter, Phys. Rev. Lett. **100**, 206001 (2008).
[3] Y. Zhu and S. Granick, Phys. Rev. Lett. **88**, 106102 (2002).
[4] T. Schmatko, H. Hervet, and L. Léger, Langmuir **22**, 6843 (2006).
[5] C. Kunert and J. Harting, Phys. Rev. Lett. **99**, 176001 (2007).
[6] U. Ulmanella and C.-M. Ho, Phys. Fluids **20**, 101512 (2008).
[7] P. A. Thompson and M. O. Robbins, Phys. Rev. A **41**, 6830 (1990).
[8] A. Jabbarzadeh, J. D. Atkinson, and R. I. Tanner, J. Chem. Phys. **110**, 2612 (1999).
[9] T. M. Galea and P. Attard, Langmuir **20**, 3477 (2004).
[10] C. Cottin-Bizonne, J.-L. Barrat, L. Bocquet, and É. Charlaix, Nat. Mater. **2**, 237 (2003).
[11] N. V. Priezjev and S. M. Troian, J. Fluid Mech. **554**, 25 (2006).
[12] P. Joseph, C. Cottin-Bizonne, J.-M. Benoît, C. Ybert, C. Journet, P. Tabeling, and L. Bocquet, Phys. Rev. Lett. **97**, 156104 (2006).
[13] C. Ybert, C. Barentin, C. Cottin-Bizonne, P. Joseph, and L. Bocquet, Phys. Fluids **19**, 123601 (2007).
[14] A. Steinberger, C. Cottin-Bizonne, P. Kleimann, and É. Charlaix, Nat. Mater. **6**, 665 (2007).
[15] J.-L. Barrat and L. Bocquet, Phys. Rev. Lett. **82**, 4671 (1999).
[16] C. Cottin-Bizonne, S. Jurine, J. Baudry, J. Crassous, F. Restagno, and É. Charlaix, Eur. Phys. J. E **9**, 47 (2002).
[17] L. Léger, J. Phys. Condens. Matter **15**, S19 (2003).
[18] M. J. Stevens, M. Mondello, G. S. Grest, S. T. Cui, H. D. Cochran, and P. T. Cummings, J. Chem. Phys. **106**, 7303 (1997).
[19] S. A. Gupta, H. D. Cochran, and P. T. Cummings, J. Chem. Phys. **107**, 10316 (1997).
[20] A. Jabbarzadeh, J. D. Atkinson, and R. I. Tanner, Trib. Int. **35**, 35 (2002).
[21] T. Schmatko, H. Hervet, and L. Leger, Phys. Rev. Lett. **94**, 244501 (2005).
[22] R. Khare, J. J. de Pablo, and A. Yethiraj, Macromolecules **29**, 7910 (1996).
[23] N. V. Priezjev and S. M. Troian, Phys. Rev. Lett. **92**, 018302 (2004).
[24] L. Kong, C. Denniston, and M. Müser, Model. Simul. Mater. SC **18**, 034004 (2010).
[25] N. V. Priezjev, A. A. Darhuber, and S. M. Troian, Phys. Rev. E **71**, 041608 (2005).
[26] S. Heidenreich, P. Ilg, and S. Hess, Phys. Rev. E **75**, 066302 (2007).
[27] J. H. Cho, B. M. Law, and F. Rieutord, Phys. Rev. Lett. **92**, 166102 (2004).
[28] O. Baumchen and K. Jacobs, J. Phys. Condens. Matter **22**, 033102 (2010).
[29] H. Sun, J. Phys. Chem. B **102**, 7338 (1998).
[30] S. Plimpton, J. Comput. Phys. **117**, 1 (1995).
[31] M. Weiss and F.-J. Elmer, Phys. Rev. B **53**, 7539 (1996).
[32] S. Lichter, A. Roxin, and S. Mandre, Phys. Rev. Lett. **93**, 086001 (2004).
[33] A. Martini, A. Roxin, R. Snurr, Q. Wang, and S. Lichter, J. Fluid Mech. **600**, 257 (2008).
[34] O. M. Braun and Y. S. Kivshar, Phys. Rep. **306**, 1 (1998).
[35] K. Falk, F. Sedlmeier, L. Joly, R. R. Netz, and L. Bocquet, Nano Lett. **10**, 4067 (2010).